



# Strategy and error analysis for machining the designed microstructured surfaces by structured grinding wheels

Amr Monier<sup>1</sup> · Bing Guo<sup>1</sup> · Qingliang Zhao<sup>1</sup> · Wenchao Liu<sup>1</sup>

Received: 10 April 2020 / Accepted: 26 November 2020 / Published online: 4 February 2021  
© The Author(s), under exclusive licence to Springer-Verlag London Ltd. part of Springer Nature 2021

## Abstract

In this research, a strategy to design structured grinding wheels to machine designed structured surfaces in *micro*-scale through the grinding process is investigated. Firstly, the geometry of the microstructured surface is defined. A mathematical model to describe the geometry of the structured grinding wheel and the grinding parameters is presented according to the geometry of the designed microstructures on the workpiece surface. And then, several operating conditions for the grinding operation are mathematically determined and kinematically simulated using a proper programming language to produce the designed geometry of the microstructured surface. The errors in the simulated geometries of the machined microstructures are calculated and analyzed. Finally, the reasons for deviation and ability to minimize error sources are investigated.

**Keywords** Grinding · Microstructured surfaces · Structured grinding wheels · Modeling · Error analysis

## List of symbols

$P$	Pitch of surface microstructures in the grinding direction ( $\mu\text{m}$ )	$N$	Number of divisions of the grinding wheel
$l_b$	Bearing width in the workpiece microstructures' pitch ( $\mu\text{m}$ )	$C$	Circumference of the 2D slice of the grinding wheel (mm)
$l_w$	Ground width in the workpiece microstructures' pitch ( $\mu\text{m}$ )	$l_n$	Circumferential distance between two consecutive grits (mm)
$h$	Microstructures height ( $\mu\text{m}$ )	$v_g$	Grinding wheel velocity (mm/s)
$P_c$	Circular pitch of wheel divisions in the circumferential direction (mm)	$v_w$	Workpiece feed rate (mm/s)
$R_g$	Radius of the grinding wheel (mm)	$v^*$	Ratio between grinding wheel velocity and workpiece feed rate
$d_g$	Groove depth in the radial direction (mm)	$d_c$	Depth of cut for grinding operation ( $\mu\text{m}$ )
$w_g$	Groove width in the circumferential direction (mm)	$\vartheta$	Slope angle of microstructures on the workpiece surface (deg)
$n$	Number of abrasive grits on a 2D wheel section	$\psi$	Helical angle of grooves on the grinding wheel surface (deg)
		$\Delta\alpha$	Angle between adjacent grits (deg)
		$\gamma_s$	Structuring ratio

✉ Bing Guo  
guobing@hit.edu.cn

Amr Monier  
amr.monier@hit.edu.cn

Qingliang Zhao  
zhaqingliang@hit.edu.cn

Wenchao Liu  
liuwc1414@163.com

<sup>1</sup> Center for Precision Engineering, School of Mechatronics Engineering, Harbin Institute of Technology, P.O. Box 413, Harbin, 150001, China

## 1 Introduction

The microstructured surface is the surface designed aiming to achieve a particular functional performance by the specific surface characteristics (structures/features) [1, 2]. For instance, it can improve the tribological and the adhesive properties of engineering components via the setting of microstructures [3–5]. In recent decades, microstructured surfaces have been widely applied in many advanced areas, such as grinding tools [6–8], engine cylinder liners [9, 10], bearings [11, 12], and seal rings [13, 14].

Different from several machining techniques of microstructured surfaces found in the literature [15–17], the grinding method of microstructured surfaces with structured grinding wheels is characterized by high efficiency and low cost. Besides, many types of regular patterns can be obtained on both hard metals and brittle materials by grinding processes, such as steel, ceramics, and cemented carbide. Figure 1a explains the principles of the microstructured surfaces grinding process with structured grinding wheels. It shows a structured wheel that is reshaped to own grooves/structures with a specific geometry. The structuring of the grinding wheel in the grinding processing is the main key for this machining method of microstructured surfaces.

Different methods have been mentioned to realize the specific geometry of grooves on grinding wheel such as diamond truer, roller truer, and laser structuring [18, 19]. Subsequently, the structured grinding wheel is used to fabricate the microstructured surfaces through the specific relative motion between the grinding wheel and the workpiece surface. Figure 1b shows typical microstructured surfaces that can be produced using this method such as straight, helical, and cross helical geometries.

Several studies have been doing on grinding of the microstructured surfaces with the structured grinding wheels aiming to optimize the process variables and improve the grinding operation. Stępień explained the principles of this grinding process for shaping different types of regular patterns on the flat and cylindrical surfaces [20]. Kinematics of the structured wheel reproduction process with different models was studied to describe the nominal workpiece

surface pattern [21, 22]. And, the effects of grinding process parameters on the geometry of the structured surface were presented [23].

Oliveira et al. [24] developed a technique that enabled the creation of different textures on the wheel surface using dressing tools with controlled external excitations. Then, these patterns could be transferred to the workpiece surface during the grinding process. Silva et al. [25, 26] used the previous methodology to innovate grinding approaches for producing workpieces with structured surfaces by grinding with low cost and practicable cycle times.

Kim et al. [27, 28] presented a simulation model for predicting ground surface patterns. They found that the grinding wheel should have a specific shape on the wheel peripheral surface and that the wheel velocity and the workpiece feed rate must be appropriate for ensuring the required grinding results. Mohamed et al. [29] performed a kinematic analysis to predict the surface structure resulting from a helically grooved grinding wheel performing the surface grinding. It was found that the groove geometry and the grinding parameters have a significant effect on the produced surface structure.

To sum up, most of the literature either tried to study the influence of geometrical/processing parameters and structures patterns of the structured wheel on the final geometry of the microstructured surfaces. Or, it aimed to predict so far the final geometry of the microstructured surfaces after the grinding operation. However, a few research work implemented the design of the structured wheels and grinding parameters based on the predesigned

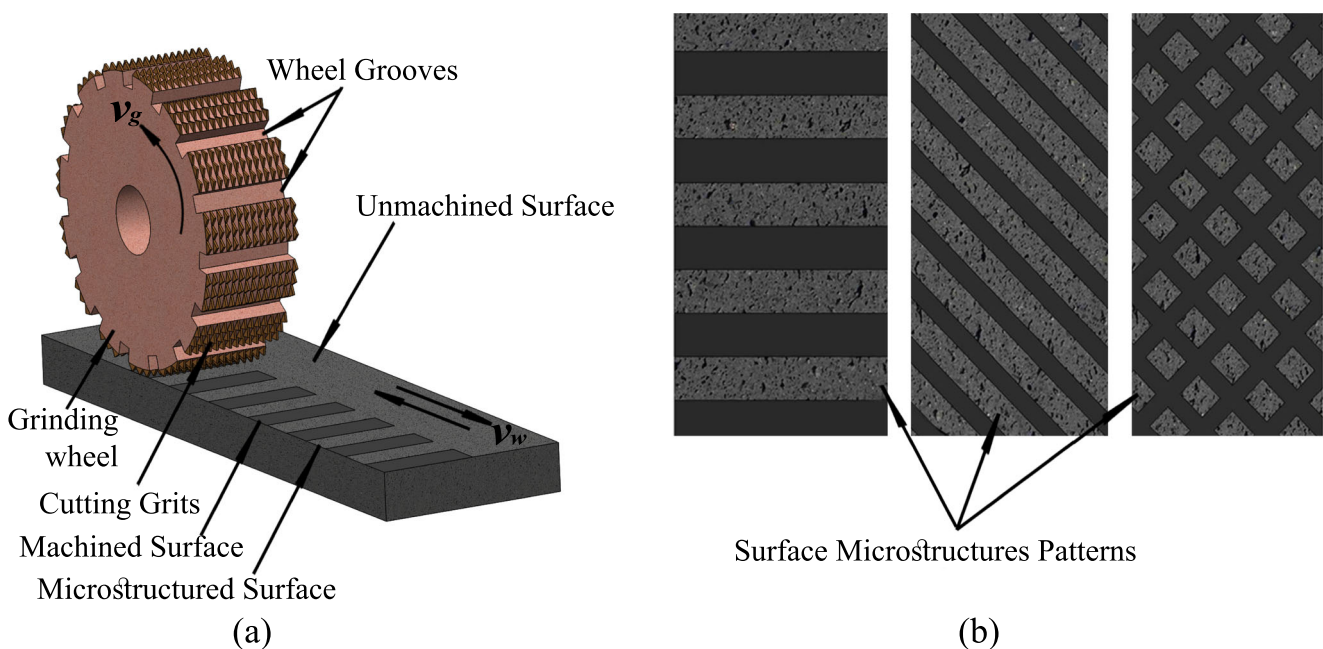


**Fig. 1** **a** A sketch explaining the principles of the microstructured surfaces grinding process with the structured grinding wheel. **b** Typical microstructured surfaces machined through the grinding process with structured grinding wheels

geometry of the microstructured surfaces before the grinding operation.

Thus, in this work, a new strategy for machining surface structures at *micro*-scale by structured grinding wheels via grinding operation is presented. It depends on designing the structured wheels and selecting the grinding parameters based on the predesigned geometry of the microstructured surfaces that is assumed as “design intent”. The investigated geometry of surface microstructures includes: the cross-section dimensions and the slope angle of microstructures on the workpiece surface. The ability to control the distance separating the microstructures over the surface is also studied. A mathematical model for the process is built. Different combinations of working parameters to get the predesigned geometry of the microstructured surface are mathematically calculated and kinematically simulated. Then, the theoretical errors in the geometries of the surface microstructures are calculated and analyzed.

## 2 Mathematical modeling for structured grinding wheels and grinding parameters to machine the designed surface features

In Fig. 2, a schematic view explains the assumptions and kinematics of the grinding strategy proposed in this work

to machine surface microstructures. Figure 2a illustrates the wheel-workpiece interaction and the process kinematics to produce surface microstructures. It shows a structured grinding wheel rotates at a grinding velocity ( $v_g$ ) and the workpiece is fed at a feed rate ( $v_w$ ). The proposed model assumes that while the grinding wheel starts moving, each grit point rolls over the workpiece surface as a summation of the rotation and translation motion through a perfect cycloidal path (see Fig. 2b).

Figure 2c explains how the microstructured surface is machined. The non-grooved grit points (green lines) machine the ground surface through the grinding operation while grooved grit points (red lines) rotate unaccompanied by machining leaving the surface features. Black segments represent the remained surface after performing the grinding operation to produce the microstructured surface shown in Fig. 2d.

The fabricated microstructure repeats itself periodically at equal distances on the workpiece surface. The distance from a point on one microstructure to the corresponding point on the next one in the longitudinal direction is named as “Pitch ( $P$ )”. As shown in Fig. 2d, every pitch consists of two parts: a ground width ( $l_w$ ), and a bearing width ( $l_b$ ). In addition to the bearing width ( $l_b$ ), the microstructure cross-section geometry has a microstructure height ( $h$ ), and a slope angle to the direction that is normal to the feed direction ( $\vartheta$ ). The geometry of surface microstructures is controlled

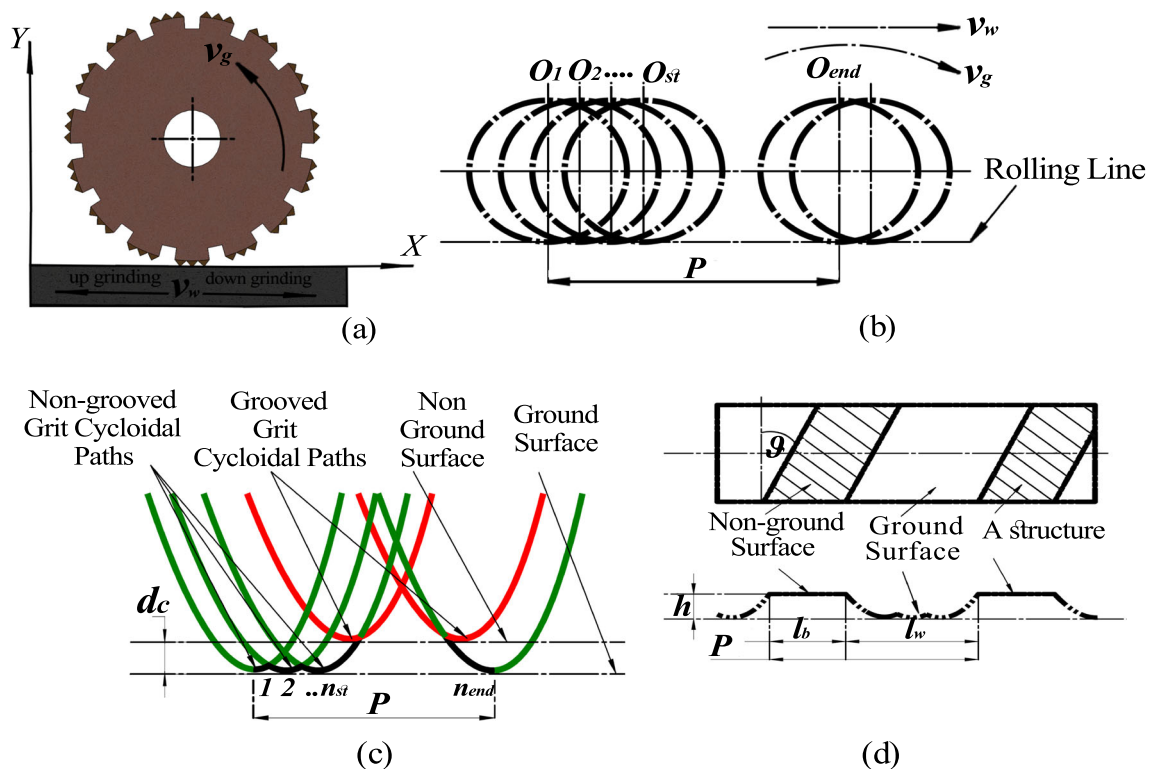


**Fig. 2** a Kinematics of the grinding process. b Rolling of the grinding wheel in cycloidal path over the workpiece surface. c Shaping of a surface feature through the motion of non-grooved and grooved grit paths within the circular pitch ( $P_c$ ). d The microstructured surface geometry

by the geometry of the structured wheel and kinematics of the grinding operation. The current strategy for machining the microstructured surface starts by designing the desired geometry of microstructures. Therefore, after calculating the values of the ground width ( $l_w$ ) and the bearing width ( $l_b$ ), the microstructures pitch ( $P$ ) can be calculated as follows:

$$P = l_w + l_b \quad (1)$$

Figure 3 explains the supposed structuring methodology for the grinding wheel. Since every feature on the workpiece surface repeats itself every pitch ( $P$ ), the model divides the surface area of the grinding wheel into a number of divisions ( $N$ ) (see Fig. 3a). Each wheel division is responsible for the formation of one feature on the workpiece surface. As shown in Fig. 3b, each wheel division contains a grooved part and a non-grooved part. The distance measured on the circumference of the grinding wheel from a point of one division to the corresponding point on the next one is termed as “circular pitch ( $P_c$ )”. The wheel’s circular pitch ( $P_c$ ) can be related to the microstructures pitch ( $P$ ) by:

$$P_c = P \cdot \frac{v_g}{v_w} = P \cdot v^* \quad (2)$$

where  $v^* = \frac{v_g}{v_w}$ , and ( $v^*$ ) is the ratio between the wheel velocity and workpiece feed rate.

Geometrical parameters of the grooves fabricated on the grinding wheel surface include the groove width ( $w_g$ ), the groove depth ( $d_g$ ), and the groove helical angle to the wheel axis ( $\psi$ ). If the percentage of the non-grooved area of a wheel division is named “structuring ratio ( $\gamma_s$ )”, then the value of the groove width ( $w_g$ ) can be given as:

$$w_g = P_c \cdot (1 - \gamma_s) \quad (3)$$

To simulate the structured grinding wheel, a wheel with radius ( $R_g$ ) is sectioned into many 2D circular sections

taken perpendicular to the wheel axis. Each section contains a number of abrasive grits ( $n$ ). All abrasive grits are assumed to be with homogeneous shape and uniformly distributed over the wheel section circumference. Figure 4 illustrates the kinematics and the model for the wheel’s 2D slice before starting up the structuring process. An abrasive grit of number ( $i$ ) is located at an angle ( $\alpha_i$ ) and radius  $r(\alpha_i)$ . The ( $\alpha_i$ ) angle defines the orientation of the  $i$ th abrasive grit and the radius  $r(\alpha_i)$  defines its radial distance from the wheel center. The maximum depth of cut ( $d_c$ ) for any grit point is assumed to be at a position where its radius is normal to the workpiece surface. The polar position of the  $i$ th grit point at any processing time is defined by an angle ( $\varphi_i$ ) referenced to that position. A single surface feature is supposed to be produced while limits of a division groove are passing normal to the workpiece surface ( $\varphi_i = \alpha_i$ ).

Figure 5 shows the limit points of a groove in a wheel division. The maximum feature height, referenced to the ground surface, depends on the polar position at which the trajectories of the groove limits are intersected in space. In Fig. 5a, the height ( $H$ ) of the intersection point can be determined by assuming that abrasive grits of the groove limits follow perfect circular paths whose centers ( $O_{L1}$  and  $O_{L2}$ ) correspond to the position of the wheel center. At the intersection point, it can be considered that while one groove limit is leaving the workpiece surface ( $\varphi_{L1} = \varphi_t$ ), the other point is engaging into the surface ( $\varphi_{L2} = -\varphi_t$ ). Radii of groove limits are assumed as the wheel radius and at a distance ( $H$ ) above the ground surface. Therefore, according to Malkin, the height of the intersection point between the limit points of wheel groove ( $H$ ) can be determined as [30]:

$$H = R_g \cdot (1 - \cos \varphi_t) \quad (4)$$

**Fig. 3** **a** The structuring methodology and geometry of the structured grinding wheel. **b** A sketch of the wheel division with the grooved and non-grooved parts

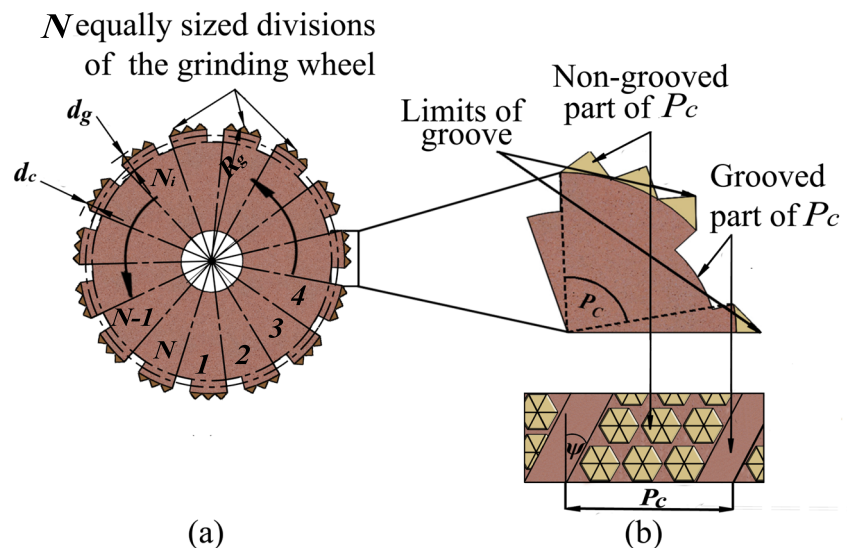
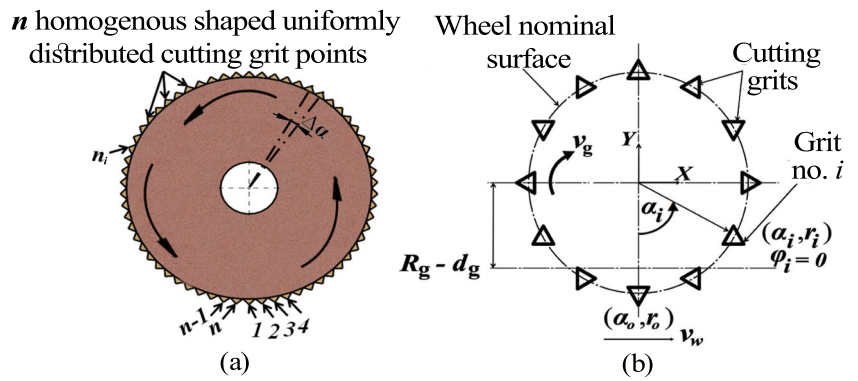


**Fig. 4** a Sketch of a non-grooved slice of the grinding wheel with  $(n)$  uniformly distributed grits. **b** Kinematic model for the grinding wheel's 2D slice



Malkin et al. [30] and Shaw et al. [31] stated that the maximum value for the cutting depth is to be equal to the grinding depth of cut ( $d_c$ ). Therefore, the feature height ( $h$ ) depends on the paths of the groove limits. The intersection between paths of limit points of a groove may occur below or above the workpiece surface as shown in Fig. 5b. Therefore, the microstructure height ( $h$ ) can be expressed as the following:

$$h = \begin{cases} H, & H < d_c \\ d_c, & d_c < H \end{cases} \quad (5)$$

Therefore, with an appropriate design for the structured grinding wheel and a proper selection of grinding parameters, the structure height ( $h$ ) can be equal to the depth of cut ( $d_c$ ) for the grinding process.

Since all abrasive grits are assumed to be uniformly distributed over the slice circumference, the angle between adjacent grits ( $\Delta\alpha$ ) can be considered equal. Then, mathematically [32]:

$$\Delta\alpha \approx \frac{2\pi}{n} \quad (6)$$

And the circumferential distance between two consecutive grits ( $l_n$ ) is given as:

$$l_n \approx 2\pi \frac{R_g}{n} \quad (7)$$

If  $C$  is the circumference of 2D slice of the grinding wheel, then:

$$C = 2\pi \cdot R_g = P_c \cdot N = l_n \cdot n \quad (8)$$

Then,

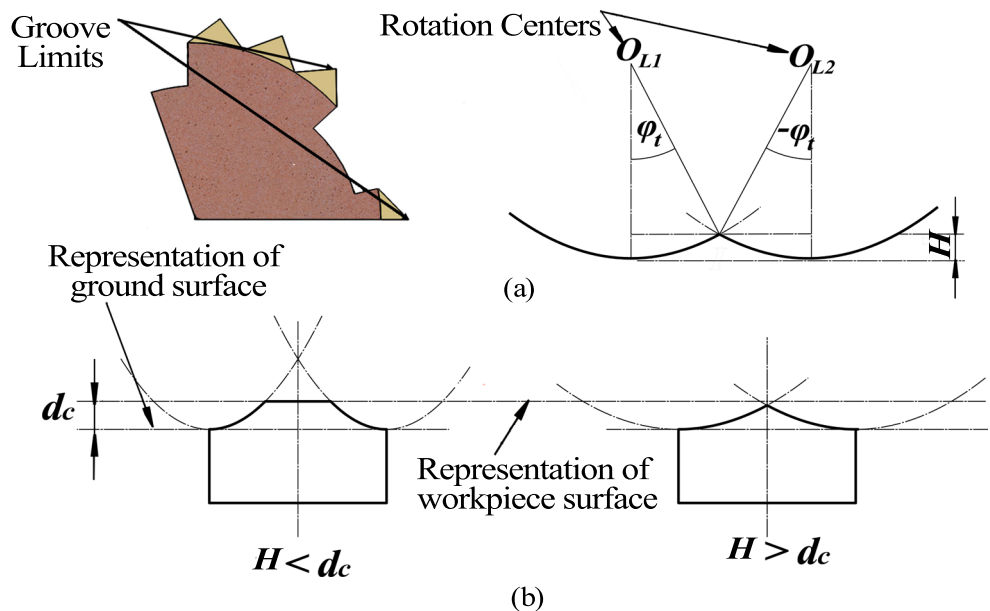
$$N = \frac{2\pi \cdot R_g}{P_c} \quad (9)$$

Assume  $n^* = \frac{n}{N}$ , then

$$n^* = \frac{P_c}{l_n} \quad (10)$$

where  $\frac{n}{N}$  ratio represents the number of abrasive grits in each circular pitch before the structuring operation. Each groove in a wheel division of number ( $N_i$ ) starts at a grit point of number ( $n_{st}$ ) and ends at ( $n_{end}$ ). The start point

**Fig. 5** a Kinematics of the groove limits to machine the feature height. **b** Sketch of the intersection point and the depth of cut ( $d_c$ )



number and the endpoint number for each groove can be calculated by:

$$n_{st} = \left[ \frac{P_C \cdot \gamma_s}{l_n} \right] \cdot N_i = \left[ \frac{n \cdot \gamma_s}{N} \right] \cdot N_i = \lceil n^* \cdot \gamma_s \rceil \cdot N_i \quad (11)$$

$$n_{end} = \left[ \frac{P_C}{l_n} \right] \cdot N_i = \left[ \frac{n}{N} \right] \cdot N_i = n^* \cdot N_i \quad (12)$$

The radial depth ( $d_i$ ) of a grit point of number ( $n_i$ ) from the wheel outer surface depends on its position over the circumference of the 2D slice and the designed groove geometrical shape. Figure 6 displays a circular pitch on the grinding wheel surface unrolled and flattened into a plane. In this figure, the variation in radial depth is plotted as a function of the grit point number in a wheel division. The geometrical shape of wheel grooves is assumed to be rectangular. For the non-grooved portion, points are assumed to be at the nominal outer surface of the grinding wheel. For the grooved portion, the depth ( $d_i$ ) is assumed constant along the groove width ( $w_g$ ) in this geometrical shape. Therefore, for rectangular-shaped grooves:

$$d_i(n_i) = \begin{cases} 0, & n_i < n_{st} \\ d_g, & n_{st} < n_i < n_{end} \end{cases} \quad (13)$$

It is suggested that the structured wheel should have grooves (straight and helical) of ( $d_g$ ) depth that is deeper than the grinding depth of cut ( $d_c$ ). Then, the radial position of each grit point can be obtained by subtracting groove depth at this point from the nominal radius of the grinding wheel as follows:

$$r_i = \begin{cases} R_g, & n_i < n_{st} \\ R_g - d_i(n_i), & n_{st} < n_i < n_{end} \end{cases} \quad (14)$$

Figure 7 shows how the geometry of the structured wheel controls the slope angle of microstructures on the workpiece surface ( $\vartheta$ ). It depicts the circular pitch ( $P_C$ ) of the grinding wheel unrolled and flattened into a plane on the up with the corresponding ground workpiece surface on the down. In this configuration, the groove is effectively a straight line forming the hypotenuse of a right-angle triangle. The corresponding straight line of the microstructure is the hypotenuse of the reflected triangle on the workpiece surface formed by the grinding operation. A side of one triangle has a length equal to the circular pitch ( $P_C$ ), while the related reflected one on the workpiece surface has a length equal to the pitch ( $P$ ) of surface microstructures. From this geometry, the helical angle ( $\psi$ ) of wheel grooves can be related to the slope angle ( $\vartheta$ ) of surface microstructures by:

$$\tan \psi = \frac{P_C}{P} \cdot \tan \vartheta. \quad (15)$$

Using Eq. (2), then

$$\tan \psi = \frac{v_g}{v_w} \cdot \tan \vartheta. \quad (16)$$

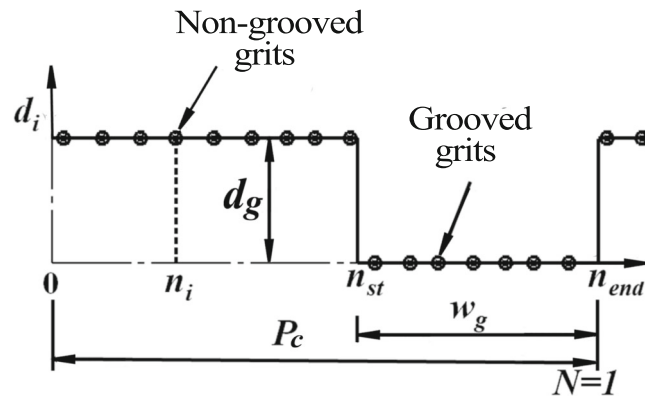


Fig. 6 Unrolled flattened view for the circular pitch ( $P_C$ ) showing its different parameters

For up grinding

$$\psi = \tan^{-1} \left[ \frac{v_g}{v_w} \cdot \tan \vartheta \right]. \quad (17)$$

For down grinding

$$\psi = 180 - \tan^{-1} \left[ \frac{v_g}{v_w} \cdot \tan \vartheta \right]. \quad (18)$$

It is clear from the previous analysis that the relation between the helical angle of wheel grooves and the slope angle of surface microstructures can be controlled by an adequate velocity ratio of the grinding process. After calculation of the circumferential and radial positions of all grit points over the wheel 2D slice, all slices are combined and the 3D shaped structured grinding wheel is created.

For each 2D slice of the wheel, the corresponding 2D profile on the workpiece is calculated. Then, all profiles are ultimately combined to form the final 3D workpiece surface. The reproduction process of the cycloidal path corresponding to the  $i$ th grit point on the workpiece surface can be determined. This is accomplished according to the time passing through the movement of that point over the surface referenced to the 0XY coordinate system connected with the workpiece. As illustrated in Fig. 8, the consumed

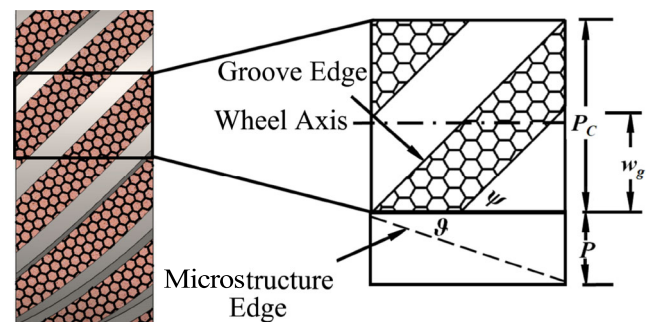
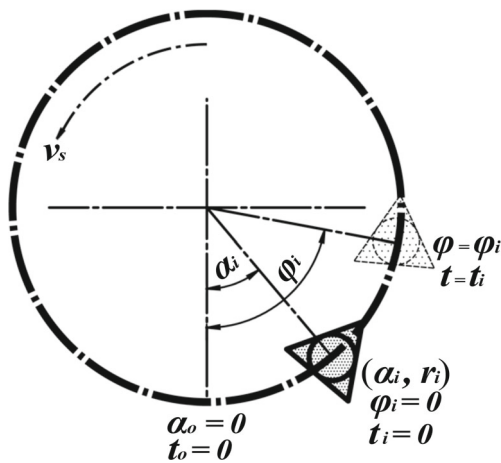


Fig. 7 The relation between the helical angle of wheel groove and the slope angle of microstructure on the machined surface



**Fig. 8** Definition of the time consumed by a grit to change its initial angular position

time by any grit to change its initial position at  $(\alpha_i)$  to be at an angular position of  $(\varphi_i)$  can be determined by:

$$t_i = \frac{r_i}{v_g} \cdot (\varphi_i - \alpha_i) \tag{19}$$

With a known engagement time, the path coordinates in the direction of the workpiece feed ( $X_i$ ) and the direction normal to the workpiece ( $Y_i$ ) can be calculated as the following:

$$\begin{cases} X_i(t) = r_i \sin \varphi_i + v_w \cdot t_i \\ Y_i(t) = -r_i \cos \varphi_i + R_g - d_g \end{cases} \tag{20}$$

Substituting Eq. (19) in to Eq. (20), then for up grinding:

$$\begin{cases} X_i(t) = r_i \sin \left( \left( \frac{v_g}{r_i} \cdot t_i \right) + \alpha_i \right) + v_w \cdot t_i \\ Y_i(t) = -r_i \cos \left( \left( \frac{v_g}{r_i} \cdot t_i \right) + \alpha_i \right) + R_g - d_g \end{cases} \tag{21}$$

For down grinding:

$$\begin{cases} X_i(t) = r_i \sin \left( \left( \frac{v_g}{r_i} \cdot t_i \right) + \alpha_i \right) - v_w \cdot t_i \\ Y_i(t) = -r_i \cos \left( \left( \frac{v_g}{r_i} \cdot t_i \right) + \alpha_i \right) + R_g - d_g \end{cases} \tag{22}$$

### 3 Obtaining the designed geometry of the workpiece surface microstructures at different sets of working conditions

The design intent of this work is to select the geometrical and processing parameters suitable for the predesigned geometry of surface microstructures. Therefore, after mathematical modeling, proper programming language is used for kinematic simulation to ensure the suitability of the determined parameters to fulfill the design intent. The mission of controlling the geometry of surface microstructures has some complexity. The structured wheel geometrical

parameters and the grinding processing parameters are interconnected and both affect the accuracy of the machined surface microstructures. Here, the deviation between the designed and simulated geometries is evaluated by “error percentages”. The tolerance deviation limit of simulated dimensions from the designed ones is assumed  $\pm 5\%$ . A negative error percentage means that the dimension is less than the designed and the positive one is higher than it.

It should be reminded that the bearing width ( $l_b$ ) value is referenced to the workpiece outer surface. It has been shown that controlling the structured wheel geometry and grinding variables makes the microstructure height ( $h$ ) approximately equal to the grinding depth of cut ( $d_c$ ) (see Fig. 5 and Eq. (5)). Therefore, the error percentages in microstructures dimensions in the following analysis are mainly accounting the deviation of bearing width ( $l_b$ ) from the designed value. There is an ability for changing different kinds of working parameters simultaneously through the kinematic simulation to figure out the microstructured surface. However, it was preferred to study the effects of each kind separately to clarify their influences on the surface.

Thus, different sets for the structured wheel geometrical parameters and grinding process parameters to obtain the cross-section dimensions and the slope angles of surface microstructures are determined and figured out. After that, results are verified through the comparison with the previous work in literature and running experiments. Dimensions and slope angles of the surface microstructures are designed and then the suitable parameters are selected. This will be explained in the following sections.

#### 3.1 Obtaining the designed cross-section dimensions of the workpiece surface microstructures at different geometries of the structured grinding wheel

This section is studying the ability to machine the cross-section dimensions of surface microstructures at different wheel geometries and the same grinding condition. Table 1 contains the cross-section dimensions of the designed surface microstructures and the grinding parameters used in this study. In designing the structured wheel, a geometry combination of the wheel parameters is assumed including: the wheel radius ( $R_g$ ), the structuring ratio ( $\gamma_s$ ), and the circular pitch ( $P_c$ ). This combination is determined

**Table 1** The designed cross-section dimensions for surface microstructures and the proposed wheel geometries

$l_b$ ( $\mu\text{m}$ )	$h$ ( $\mu\text{m}$ )	$d_c$ ( $\mu\text{m}$ )	$v^*$	$R_g$ (mm)
20	20	20	30	5 10 15 20 25

simultaneously to obtain the predesigned geometry of surface microstructures. After calculating the values for this combination, complete design for the grooved wheel geometry can be achieved. In this work, the number of wheel divisions ( $N$ ) is determined relative to the circular pitch ( $P_c$ ) value (see Eq. (9)). Structured wheels with different geometries suitable to machine the designed geometry of surface microstructures are determined mathematically at each assumed radius in Table 1. The calculated parameters are visualized through kinematic simulation using programming languages.

Figure 9a explains the relation between the structuring ratio ( $\gamma_s$ ) and circular pitch ( $P_c$ ) at each wheel radius ( $R_g$ ) to machine the designed cross-section dimensions of surface microstructures. Using the values mentioned in Table 1, a range of suitable values for the structuring ratios and the corresponding circular pitches are calculated mathematically and then kinematically simulated. The continuous black solid lines represent the analytical values for wheels' geometries, while the blue points represent the simulated geometrical conditions to satisfy the design intent of this section. To keep the dimensions of surface microstructures constant while the wheel geometry is changing, a positive correlation between the circular pitch ( $P_c$ ) and the structuring ratio ( $\gamma_s$ ) is figured out at the same wheel radius ( $R_g$ ).

Figure 10 shows one solution for the grooved wheel geometry and the corresponding structured surface at each wheel radius mentioned in Table 1. Table 2 includes the resultant values for geometries of the simulated structured wheels and microstructured surfaces shown in Fig. 10. The microstructures dimensions simulated at different wheels geometries are very close to the designed dimensions (20  $\mu\text{m}$  by 20  $\mu\text{m}$ ) and uniformly repeated over the surface. So, the design intent of this section can be considered to be obtained.

The error percentage in the bearing width ( $l_b$ ) obtained at each condition represented as a blue point in Fig. 9a is shown in Fig. 9b as a red point. The value of error percentage

**Table 2** Geometries of the simulated structured grinding wheels and microstructured surfaces

$R_g$ (mm)	$\gamma_s$	$N$	$P$ ( $\mu\text{m}$ )	$l_w$ ( $\mu\text{m}$ )	$l_b$ ( $\mu\text{m}$ )	$h$ ( $\mu\text{m}$ )
5.00	0.76	5	209.40	189.50	19.90	20.00
10.00	0.46	18	116.30	96.10	20.20	20.00
15.00	0.45	24	130.90	110.80	20.10	20.00
20.00	0.56	23	182.10	162.10	20.00	20.00
25.00	0.75	15	349.00	328.80	20.20	20.00

might be repeated at different geometrical conditions. Therefore, the number of blue points in Fig. 9a and red points in Fig. 9b at each wheel radius may be not the same. All error percentages of simulated widths for microstructures are in range  $\pm 5\%$ . The represented heights are equal to the grinding depth of cut ( $d_c$ ) mentioned in Table 1. Therefore, the error percentages in simulated heights of microstructures are not existent.

Although error percentages figured out in Fig. 9b are in the assumed tolerance range, their source can be explained. In the kinematic simulation, only geometrical values of wheel parameters that make the number of wheel divisions ( $N$ ) integer are accepted. Also, grinding wheel radii are kept as designed such as stated in Table 1. Axes resolution in kinematic simulation also affects the accuracy of the results. Therefore, some modifications are done to the analytical values of the wheel's geometries causing some changes in the bearing widths. To minimize or eliminate error percentages, the velocity ratio ( $v^*$ ) should be modified.

The previous results and explanations for changing the selected geometrical parameters to preserve the geometry of designed surface microstructures constantly agreed with the principles explained by Malkin et al. [30] and Shaw et al. [31] and the work published by Mohamed et al. [29] on the effects of parameters of the grooved grinding wheel on the geometry of the structured surfaces. According to the principles of Malkin et al. [30] and Shaw et al. [31], with the

**Fig. 9** **a** Geometrical combinations to machine the cross-section dimensions of surface microstructures. **b** Error percentages between the designed and the simulated microstructures ground width ( $l_b$ )

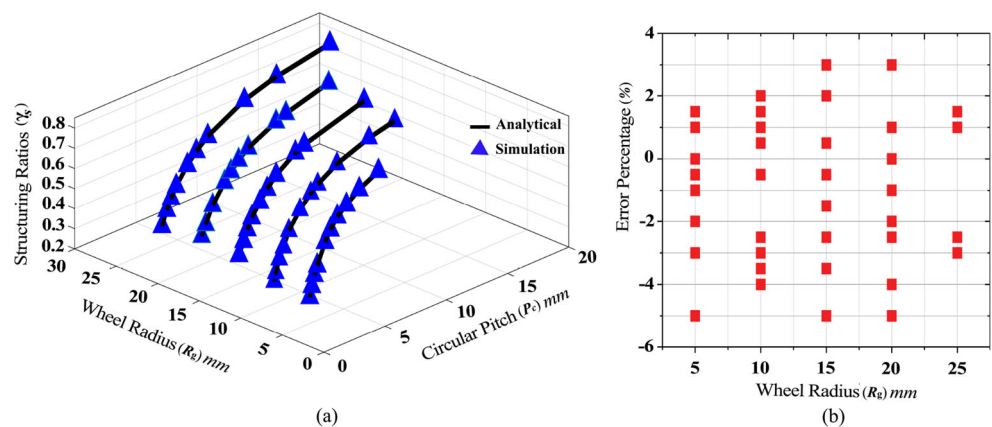
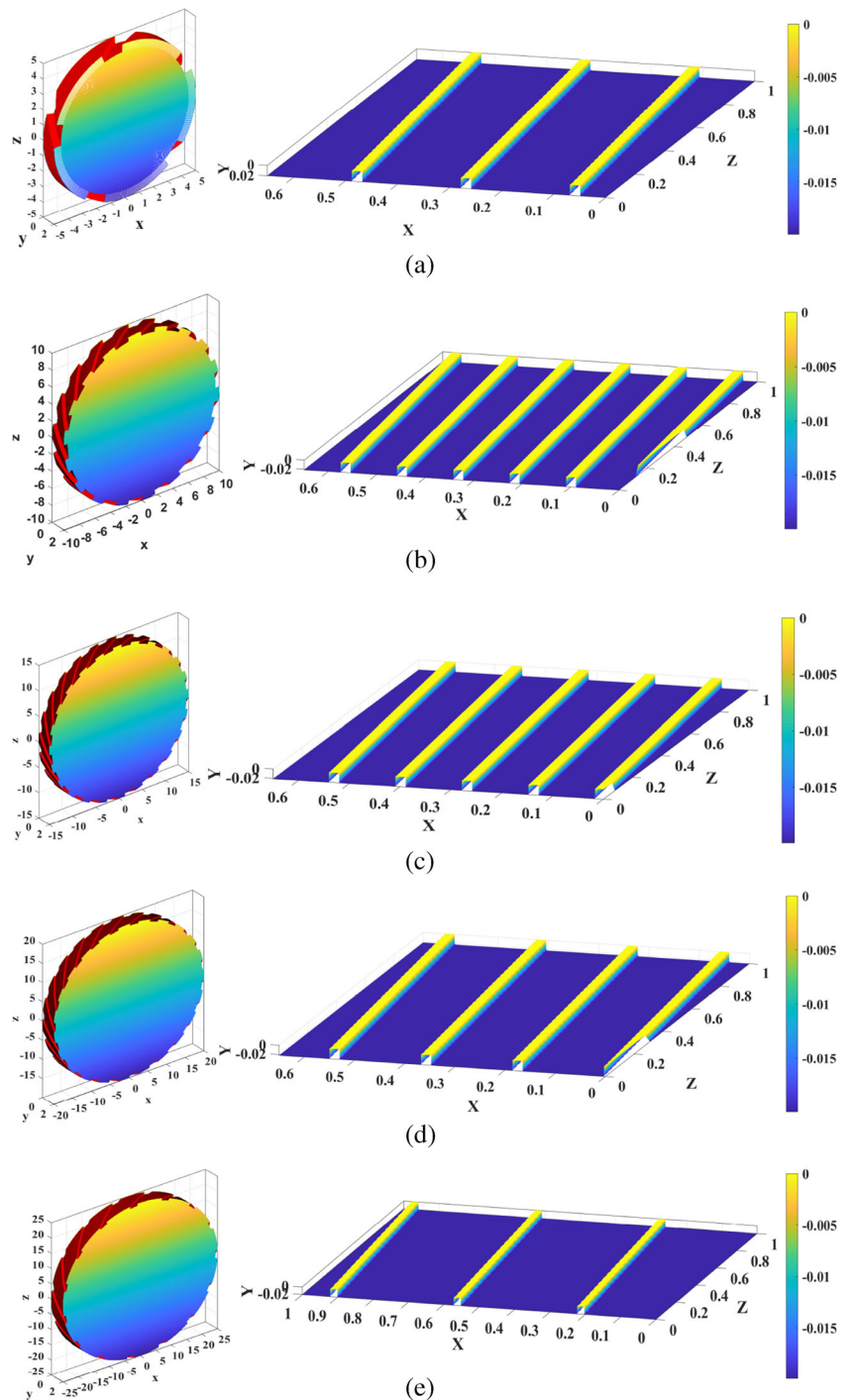




**Fig. 10** Simulation of the machined microstructures on the ground surface at different geometrical combinations of the structured grinding wheels



increasing wheel radius, the value of microstructure width decreases due to the increase in contact length between the wheel and workpiece surfaces. Besides, Mohamed et al. [29] showed that with the increasing percentage of the non-removed area (structuring ratio) of the wheel surface, the structure width decreases. Consequently, according to these behaviors, the varying wheel geometrical parameters can be recalculated and reselected to fulfill the design intent with the changing wheel geometry.

### 3.2 Obtaining the designed cross-section dimensions of the workpiece surface microstructures at different processing parameters for the grinding operation

In this section, the ability to machine the cross-section dimensions of surface microstructures at different grinding conditions with the same wheel geometry is studied. Table 3 contains the cross-section dimensions of the designed

**Table 3** The designed cross-section dimensions for surface microstructures and the proposed grinding parameters

$l_b$ ( $\mu\text{m}$ )	$h$ ( $\mu\text{m}$ )	$d_c$ ( $\mu\text{m}$ )	$R_g$ (mm)	$\gamma_s$	$v^*$
20	20	20	25	0.50	35 85 130 160 200

surface microstructures and the grinding parameters used in this section. Different velocity ratios for grinding operation are investigated while the grinding depth of cut ( $d_c$ ) is assumed equal to the designed microstructure height ( $h$ ).

Figure 11 explains the relation between the velocity ratio ( $v^*$ ) and the circular pitch ( $P_c$ ) to machine the designed cross-section dimensions of surface microstructures which are listed in Table 3. Likewise, the continuous black solid line represents the analytical calculations and the blue points represent the simulated grinding conditions to satisfy the design intent of this study. A directly proportional relationship between the velocity ratio ( $v^*$ ) and the circular pitch ( $P_c$ ) is represented to get the dimensions of surface microstructures as designed.

Figure 12 shows the simulated microstructured surfaces and the corresponding structured wheels at different grinding conditions listed in Table 3. As shown in Fig. 12, the velocity ratio ( $v^*$ ) can control the cross-section dimensions and the separating distance over the machined surface. Table 4 contains the resultant geometries of simulated microstructured surfaces which are shown in Fig. 12 at each working condition. Microstructures dimensions simulated at the different grinding conditions can be assumed to be as the designed ones and uniformly distributed over the surface.

Although the change in velocity ratio ( $v^*$ ) should be followed by variation in the circular pitch ( $P_c$ ) to make microstructures dimensions constant. However, this change did not be considered as a geometrical change. On one hand, the circular pitch ( $P_c$ ) is determined relative to the wheel

radius ( $R_g$ ) and the structuring ratio ( $\gamma_s$ ) that are set fixed during this study. Furthermore, for a single grooved wheel, one geometry condition at suitable processing parameters to machine the dimensions of the designed microstructures can satisfy the design intent.

Error percentages in bearing widths simulated at each working condition (blue point) in Fig. 11a are shown in Fig. 11b. It is shown that the simulated microstructures widths are very close to the designed value and the microstructure heights ( $h$ ) are equal to the grinding depth of cut ( $d_c$ ) stated in Table 3. Thus, errors in microstructures heights do not exist. It can be noted that, although the sources of “error percentage” explained in the previous section, error values in Fig. 11b are smaller compared to those found in Fig. 9b. This can be explained as controlling grinding conditions and modifying them is more familiar than changing the geometry of the structured grinding wheel.

These results and explanations of the changing geometry of surface microstructures with the changing processing parameters are agreed to the work done by Stępień [23]. He stated that when the velocity ratio ( $v^*$ ) is very large, structures on the workpiece surface in successive rotations of the wheel do not separate. Additionally, the workpiece feeds should be greater than the lower critical value.

### 3.3 Obtaining the designed slope angle of the workpiece surface microstructures at different wheel geometries and/or grinding parameters

In addition to cross-section dimensions, the geometry of surface microstructures includes the designed orientation. From the mathematical model, microstructures slope angle ( $\vartheta$ ) can be obtained either at a constant velocity ratio ( $v^*$ ) and structured grinding wheels grooved at a specific value of the helical angle ( $\psi$ ). Or, it can be machined with a grinding wheel grooved at a specific helical angle ( $\psi$ ) and

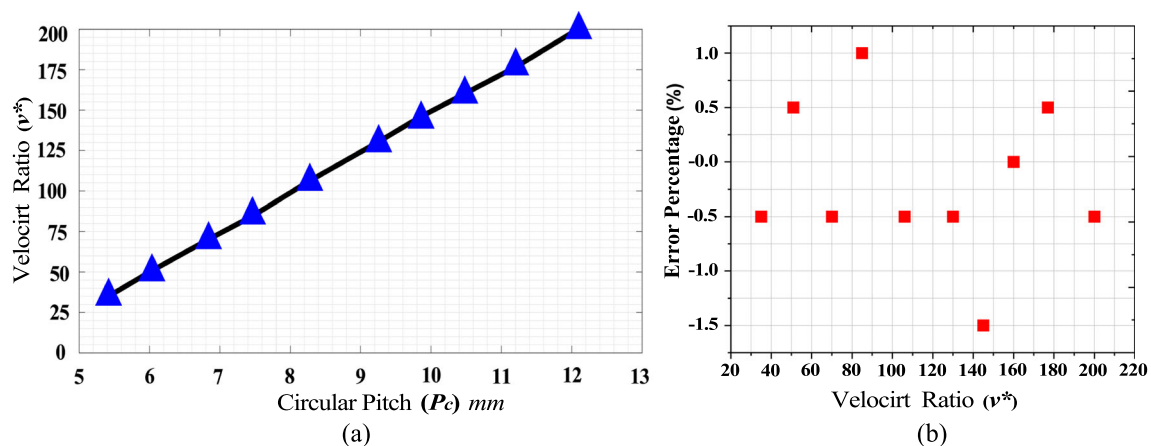


**Fig. 11** Analytical and simulated velocity ratios to machine the cross-section dimensions of surface microstructures. **b** Error percentages between the designed and the simulated microstructures ground width ( $l_b$ )

**Fig. 12** Simulation of the machined microstructures on the ground surface at different velocity ratios

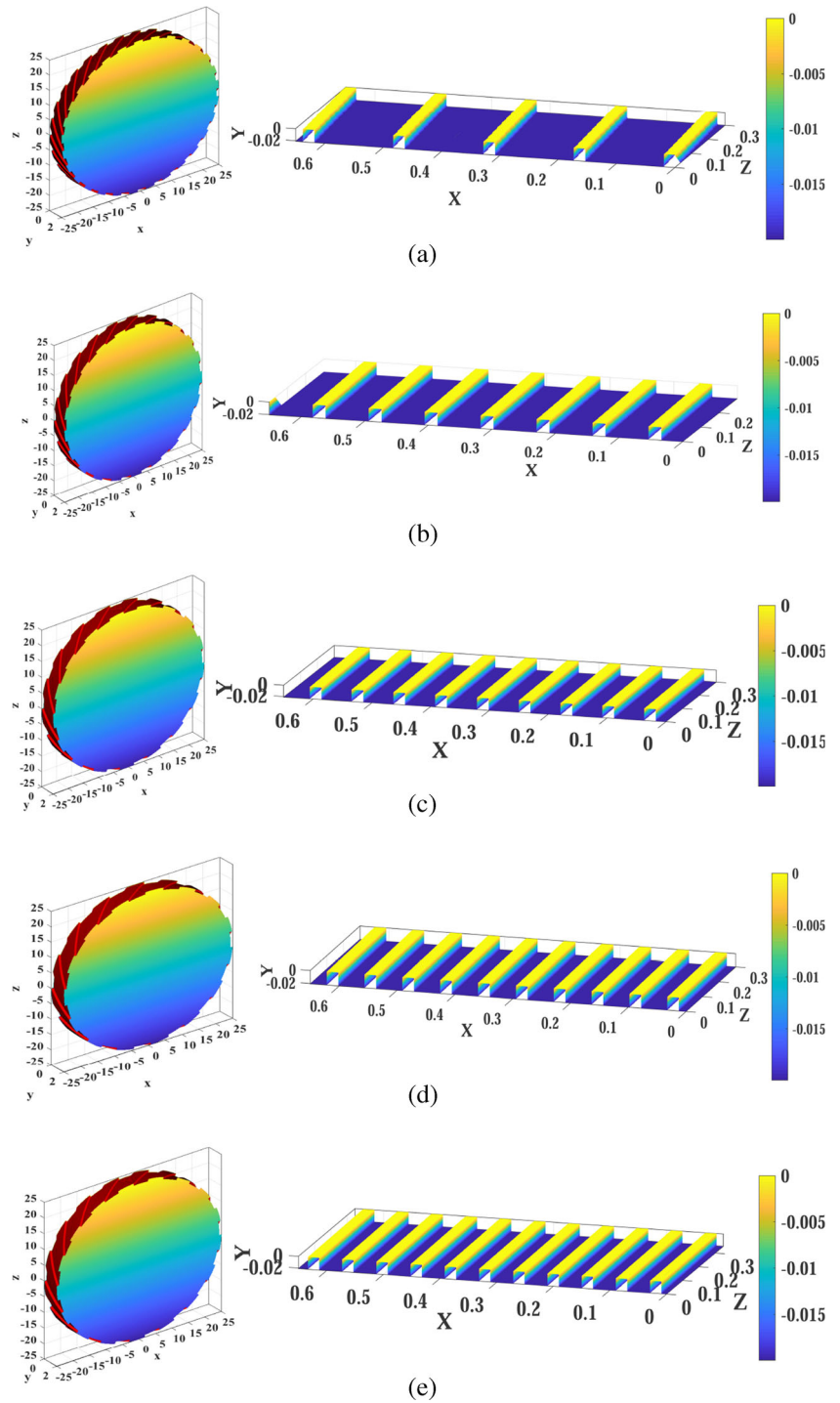


**Table 4** Grinding conditions and geometries of the simulated microstructured surfaces

$v^*$	$N$	$P$ ( $\mu\text{m}$ )	$l_w$ ( $\mu\text{m}$ )	$l_b$ ( $\mu\text{m}$ )	$h$ ( $\mu\text{m}$ )
35	29	154.70	134.80	19.90	20.00
85	21	88.00	67.80	20.20	20.00
130	17	71.10	51.20	19.90	20.00
160	15	65.50	45.50	20.00	20.00
200	13	60.40	40.50	19.90	20.00

**Table 5** The designed microstructures geometry and the proposed geometrical and processing variables to get the required slope angle

$l_b$ ( $\mu\text{m}$ )	$h$ ( $\mu\text{m}$ )	$d_c$ ( $\mu\text{m}$ )	$v^*$	$\psi$ (deg)
20	20	20	30	69°
				83°
				87°

a determined velocity ratio ( $v^*$ ) (Eqs. (15)–(18)). Therefore, after designing the required value for the microstructures slope angle on the workpiece surface, the convenient way is determined to fulfill the design intent.

Table 5 contains the geometrical and processing parameters used to get the microstructured surface dimensions with slope angles of 5°, 15°, and 30°. The corresponding helical angles for the structured wheels calculated mathematically are 69°, 83°, and 87° respectively. Figure 13 exhibits the structured wheels with the determined helical angles and the designed geometry of surface microstructures listed in Table 5.

The required microstructures' slope angles can also be obtained with the same structured wheel angle ( $\psi$ ) but at different velocity ratios (see Fig 14). Using a structured wheel with a helical angle ( $\psi$ ) of 60°, velocity ratios of 19.80, 6.47, and 3.00 are suggested mathematically to obtain structures with slope angles of 5°, 15°, and 30° respectively. As the velocity ratio changes, the dimensions of the microstructure will change as well. Therefore, as

shown in Fig. 14, the designed slope angles of surface microstructures are obtained but with different cross-section dimensions than that mentioned in Table 5. If surface microstructures are needed to be machined at the designed dimensions of Table 5, the circular pitch ( $P_c$ ) of the structured grinding wheel should be modified (see Fig. 11a).

Mathematically calculated values for the helical angles of the structured grinding wheels and the velocity ratios can be used in kinematic simulation without any modifications. Therefore, error percentages in slope angles of the simulated surface microstructures in Figs. 13 and 14 do not exist. Slope angles of microstructures can optimize the required length of machined structures over the workpiece surface according to the application and the design intent.

The behavior of the surface microstructures inclination is consistent with the previous work studied by Mohamed et al. [29]. He showed that the slope angle of surface structure changes with the change of the working velocities for the grinding wheel and the workpiece.

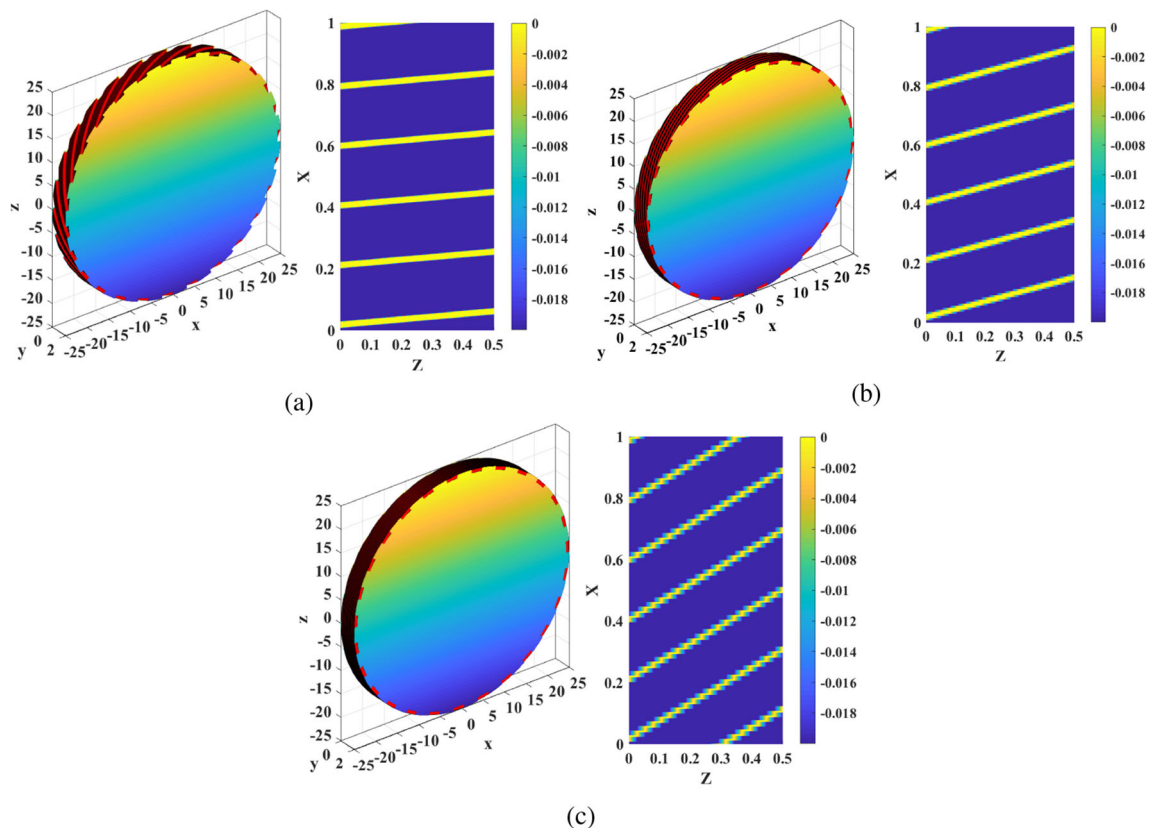
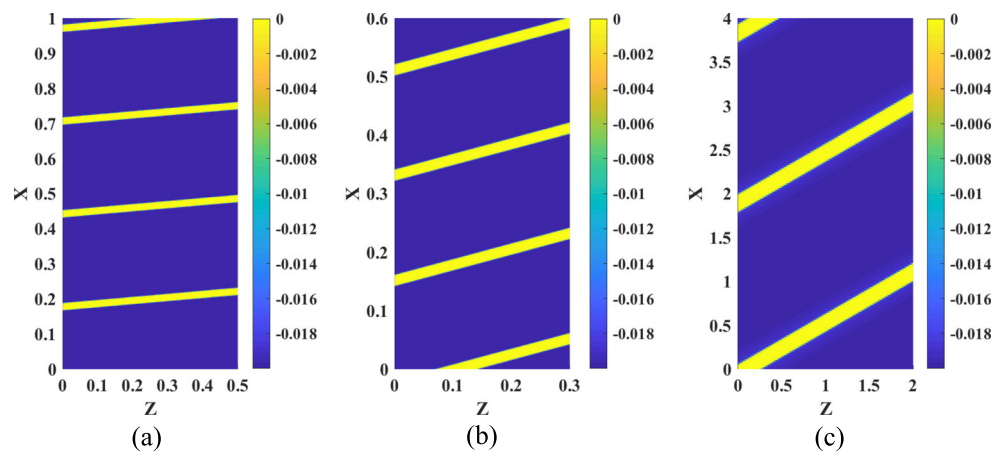


**Fig. 13** Machining of the microstructures slope angles at different helical angles for the structured grinding wheels

**Fig. 14** Machining of the microstructures slope angles at different velocity ratios



**3.4 Experimental verification of results**

In order to investigate the ability of the presented model to satisfy the design intent and machine the microstructured surfaces, initial grinding operations were executed. A structured grinding wheel was used for performing the grinding operations on tungsten carbide specimens at different working conditions. The obtained machined surfaces were evaluated and the difference in simulated and experimental dimensions was calculated. As mentioned before, the difference in the dimensions is mainly accounted for the bearing width ( $l_b$ ). Figure 15 shows the geometry of the structured grinding wheel used in the grinding operations. Table 6 contains the values for the resultant simulated and experimental geometries of the microstructured surfaces machined at different working conditions. Also, the error percentages at each working condition are also included. Figure 16 shows the simulated and machined microstructured surfaces at the listed working conditions. There is an agreement between the pictures and the measured values of the simulated and experimental microstructured surfaces.

**4 Discussion**

Dimensions of surface microstructures can be machined at different structured wheels geometries. At a constant wheel radius, increasing the circular pitch ( $P_c$ ) increases the microstructures’ pitch ( $P$ ) on the workpiece surface per unit partition of the wheel divisions (see Eq. (2)). This is achieved through increasing in both ground and bearing widths ( $l_w$  and  $l_b$ ). To retain the bearing width ( $l_b$ ) value constant equal to the designed one, this should be compensated by increasing the structuring ratio ( $\gamma_s$ ). This increases the percentage of the cutting area of the wheel segment by reducing the groove width ( $w_g$ ) of the wheel division (see Eq. (3)). Therefore, the increase in the microstructures’ pitch ( $P$ ) with the increasing circular pitch ( $P_c$ ) is achieved by raising the ground width ( $l_w$ ) value keeping the bearing width ( $l_b$ ) value approximately constant.

On the other side, raising the wheel radius does not affect the separating distance between surface microstructures (see Eq. (2)). Rather, this increases the contact zone

**Fig. 15** Geometry of the structured wheel used during the experiments ( $R_g = 25$  mm and  $\gamma_s = 0.50$ )

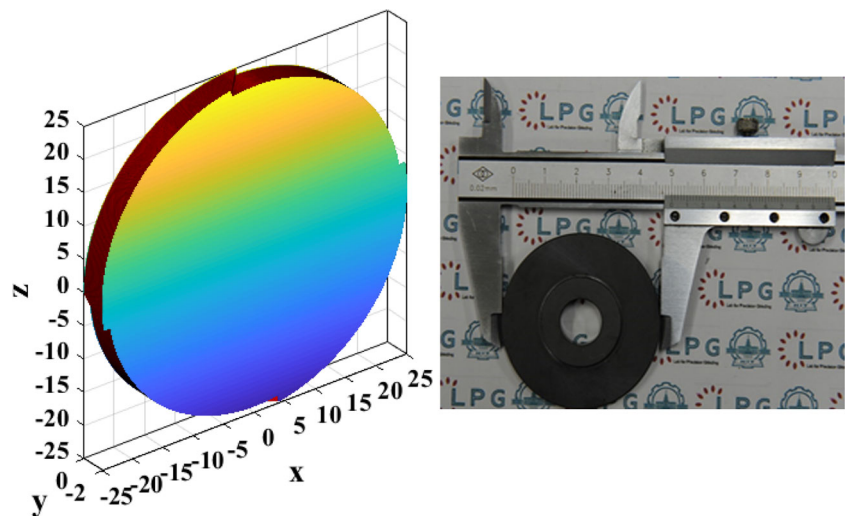


**Table 6** Grinding conditions and geometries of the simulated microstructured surfaces

Condition No.	Simulated bearing width $l_b$ ( $\mu\text{m}$ )	Experimental bearing width $l_b$ ( $\mu\text{m}$ )	Error percentage (%)
a	255	220	15.91
b	300	310	3.23
c	450	440	2.27
d	410	380	7.89

between the wheel and the workpiece surface. Therefore, the ground width ( $l_w$ ) of the microstructures' pitch ( $P$ ) increases and the cutting paths of the groove limits overlap at the same cutting area. After that, the bearing width ( $l_b$ )

at the workpiece outer surface is sheared and completely disappears. Besides, the microstructure height is continuing to decrease due to the increasing value for the intersection point of the groove limits below the surface as explained

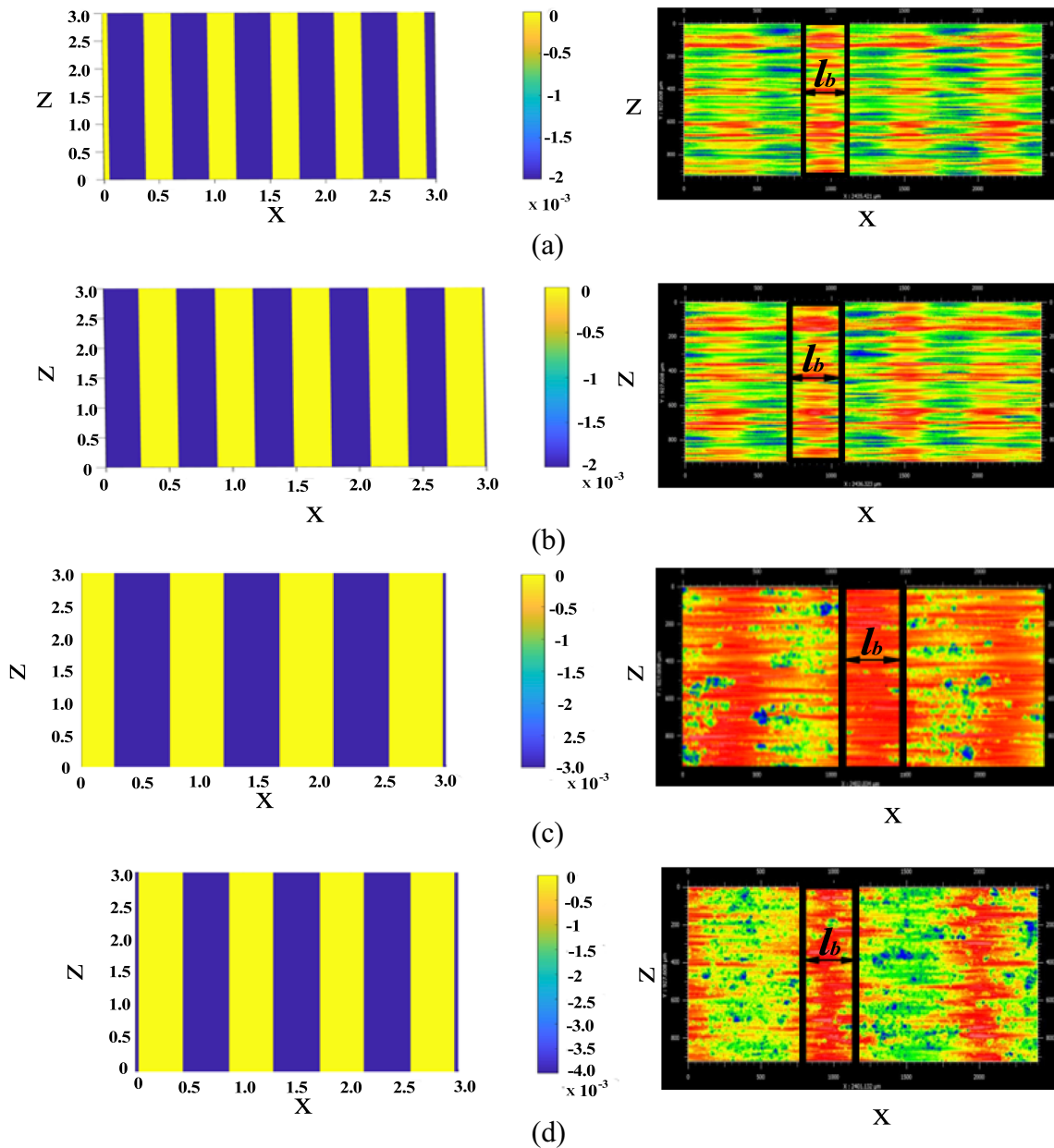


**Fig. 16** Simulated and machined microstructured surfaces obtained at different working conditions

in Fig. 5. This can be dealt by recalculation of the circular pitch ( $P_c$ ) and the structuring ratio ( $\gamma_s$ ) to be compatible with the selected wheel radius ( $R_g$ ). Hence, the difference between the resulted pitch ( $P$ ) and the ground width ( $l_w$ ) of microstructures on the machined surface remains constant. Therefore, the bearing width ( $l_b$ ) keeps its value as designed (see Eq. (1)). As a result, the separation between surface microstructures is achieved leaving parts of the workpiece outer surface free of machining. Then, the designed bearing width ( $l_b$ ) and height ( $h$ ) of microstructures can be achieved equal to the designed ones at the allowed tolerance (see Fig. 10).

This method seems to be effective in controlling the separating distance between microstructures and the number of features over the microstructured surface. If the number of features per unit length is defined as microstructures linear density or in short “microstructures density”. Then, adequate calculations of the pitch ( $P$ ) and the ground width ( $l_w$ ) can control microstructures density. This way can improve the functionality of surface structuring and maximize its effect on engineering parts.

In addition, to keep the dimensions of the microstructures constant while the velocity ratio ( $v^*$ ) is changing, the circular pitch ( $P_c$ ) should be modified. As the increase in the velocity ratio ( $v^*$ ) means increasing the wheel velocity relative to the workpiece feed rate. Therefore, the microstructures pitch ( $P$ ) decreases with the increasing velocity ratio ( $v^*$ ) (see Eq. (2)). This behavior makes the paths of the groove limits overlap the same cutting area. Consequently, it leads to the disappearing of the bearing width ( $l_b$ ) at the workpiece outer surface and decreasing of the microstructure height ( $h$ ). Hence, the separation between surface microstructures cannot be realized. To solve this matter, the circular pitch ( $P_c$ ) should be modified to allow increasing the swept distance per unit wheel division (see Eq. (2)). Then, the separation between the surface microstructures is obtained and the designed microstructures’ cross-section dimensions are obtained (see Fig. 5 and Eq. (5)).

## 5 Conclusion

In this paper, a strategy for production surface structures in *micro*-scale using structured grinding wheels is proposed. Controlling the geometry of surface microstructures is investigated. Different parameters participating in the process are studied. The conclusions are as follows:

1. Machining of pre-designed geometry for microstructured surfaces with specific dimensions and orientation using structured grinding wheels can be mathematically formulated and simulated. Different sets of variables

like wheel radii, structuring ratios, velocity ratios, and groove angles can be selected according to availability to achieve the design intent.

2. To obtain microstructures with a defined geometry, the geometrical and processing parameters should be selected properly to achieve separation between surface microstructures.
3. In the designing and parameters selection stage, it should be taken into account that the change in the separating distance between microstructures should be achieved by changing the ground width keeping the bearing width as the designed value.
4. At a constant speed ratio, the structuring ratio and the circular pitch should be fit with the wheel radius to prevent the duplication of the cutting process over the same area and allow the separation between surface microstructures.
5. The velocity ratio has a major effect on structures dimensions and the slope angle of surface microstructures.
6. Error percentages that appear on geometry of simulated surface microstructures can be analyzed and compensated.

**Acknowledgments** Special thanks to Mr. Jun Zhang for his support and assistance during doing the experiments.

**Funding** This work was supported by the National Natural Science Foundation of China (Grant No.: 51875135) and National Natural Science Foundation of Heilongjiang Province (Grant No.: E2018037).

## References

1. Bruzzone AAG, Costa HL, Lonardo PM, Lucca DA (2008) Advances in engineered surfaces for functional performance. *CIRP Ann* 57(2):750–769
2. Evans CJ, Bryan JB (1999) “Structured”, “textured” or “engineered” surfaces. *Cirp Ann* 48(2):541–556
3. Zhang XH, Kang ZX, Li S, Wu QP, Zhang ZC (2018) Experimental investigations on the impact of different laser macro-structured diamond grinding wheels on alumina ceramic. *Int J Adv Manuf Tech* 96(5-8):1959–1969
4. Deng H, He J (2017) A study of the grinding performance of laser micro-structured coarse-grained diamond grinding wheels. *Int J Adv Manuf Tech* 93(5-8):1989–1997
5. Chen CS, Tang JY, Chen HF, Bo Z (2018) An active manufacturing method of surface micro structure based on ordered grinding wheel and ultrasonic-assisted grinding. *Int J Adv Manuf Tech* 97(5-8):1627–1635
6. Deng H, Zhou X (2019) Dressing methods of superabrasive grinding wheels: a review. *J Manuf Process* 45:46–69
7. Zhang X, Wen D, Shi Z, Si L, Kang Z, Jiang J, Zhang Z (2020) Grinding performance improvement of laser micro-structured silicon nitride ceramics by laser macro-structured diamond wheels. *Ceram Int* 46(1):795–802
8. Zhang X, Kang Z, Si L, Shi Z, Wen D, Jiang J, Zhang Z (2019) Grinding force modelling for ductile-brittle transition in laser

- macro-micro-structured grinding of zirconia ceramics. *Ceram Int* 45(15):18487–18500
9. Willis E (1986) Surface finish in relation to cylinder liners. *Wear* 109(1-4):351–366
  10. Sabri L, El Mansori M (2009) Process variability in honing of cylinder liner with vitrified bonded diamond tools. *Surf Coat Technol* 204(6-7):1046–1050
  11. Tala-Ighil N, Fillon M, Maspeyrot P (2011) Effect of textured area on the performances of a hydrodynamic journal bearing. *Tribol Int* 44(3):211–219
  12. Brizmer V, Kligerman Y, Etsion I (2003) A laser surface textured parallel thrust bearing. *Tribol Trans* 46(3):397–403
  13. Pawlus P, Galda L, Dzierwa A, Koszela W (2009) Abrasive wear resistance of textured steel rings. *Wear* 267(11):1873–1882
  14. Zhang F, Meng B, Geng Y, Zhang Y, Li Z (2016) Friction behavior in nanoscratching of reaction bonded silicon carbide ceramic with berkovich and sphere indenters. *Tribol Int* 97:21–30
  15. Li HN, Yang Y, Zhao YJ, Zhang Z, Zhu W, Wang W, Qi H (2019) On the periodicity of fixed-abrasive planetary lapping based on a generic model. *J Manuf Process* 44:271–287
  16. Zhang F, Meng B, Geng Y, Zhang Y (2016) Study on the machined depth when nanoscratching on 6h-sic using berkovich indenter: Modelling and experimental study. *Appl Surf Sci* 368:449–455
  17. Guo B, Zhao Q, Xin Y (2014) Surface micro-structuring of coarse-grained diamond wheels by nanosecond pulsed laser for improving grinding performance. *Int J Pr Eng Manuf* 15(10):2025–2030
  18. Tawakoli T, Daneshi A (2013) New kinematic in dressing of grinding wheels. In: *ASME International mechanical engineering congress and exposition*, vol. 56192, pp V02BT02A076. American Society of Mechanical Engineers
  19. Wu M, Guo B, Zhao Q, He P (2018) Precision grinding of a microstructured surface on hard and brittle materials by a microstructured coarse-grained diamond grinding wheel. *Ceram Int* 44(7):8026–8034
  20. Stępień P, Maciej Szafarczyk (1989) Generation of regular patterns on ground surfaces. *CIRP Ann* 38(1):561–566
  21. Stępień P (2007) Undeformed chip sizes in grinding process of regular surface texture generation. *Arch Mech Eng* 54(3):235–259
  22. Stępień P (2011) Deterministic and stochastic components of regular surface texture generated by a special grinding process. *Wear* 271(3-4):514–518
  23. Stępień P (2009) Regular surface texture generated by special grinding process. *J Manuf Sci Eng* 131(1):011015-1011015-7
  24. Oliveira JFG, Bottene AC, Franca TV (2010) A novel dressing technique for texturing of ground surfaces. *CIRP annals* 59(1):361–364
  25. Silva EJ, Bottene AC, de Oliveira JFG, Atoatte A, de Souza Rodrigues A (2016) Grinding process for profiled texturing. *CIRP Ann* 65(1):337–340
  26. da Silva EJ, de Oliveira JFG, Salles BB, Cardoso RS, Reis VRA (2013) Strategies for production of parts textured by grinding using patterned wheels. *CIRP Ann* 62(1):355–358
  27. Kim H, Ko TJ (2014) Simulation of micro-patterns engraved by grinding process with screw shaped wheel. *Simul Model Pract Theory* 49:277–286
  28. Kim HC, Ko TJ (2015) Verification of simulation of surface texturing on planar surface by grinding. *Int J Precis Eng Manuf* 16(2):225–231
  29. Mohamed ALMO, Warkentin A, Bauer R (2017) Prediction of workpiece surface texture using circumferentially grooved grinding wheels. *Int J Adv Manuf Technol* 89(1-4):1149–1160
  30. Malkin S, Guo C (2008) *Grinding technology: theory and application of machining with abrasives*. Industrial Press Inc.
  31. Shaw MC (1996) *Principles of abrasive processing*. Number 13 Oxford University Press on Demand
  32. Bruce EM (2014) *Fundamental concepts of geometry*. Courier Corporation

**Publisher's note** Springer Nature remains neutral with regard to jurisdictional claims in published maps and institutional affiliations.